**Supplemental Materials**

# Governing role of the ratio of large platelet particles to ultrafine particles on dynamic and quasistatic compressive response and damage evolution in ice-templated alumina ceramics

Mahesh Banda, Sashanka Akurati, *Dipankar Ghosh

Department of Mechanical and Aerospace Engineering
Old Dominion University, Norfolk, VA 23529, USA

*Corresponding author (D. Ghosh): Phone: +1-757-683-3738; Fax: +1-757-683-5344; E-mail address: dghosh@odu.edu

**Preparation of aqueous alumina suspensions and ice-templating procedure**

Aqueous suspensions were prepared by mixing the required amount of deionized (DI) water and UA and PA particles. Ammonium polymethacrylate (Darvan C, R.T. Vanderbilt Co., Norwalk, CT), in the proportion of 1 wt.% of total solid loading (ceramic content), was used as a dispersant in the aqueous suspensions. DI water, dispersant, UA powder, and zirconia ($ZrO_2$, 5 mm in diameter) grinding media was taken to a Nalgene bottle and jar milled for 24 hours. For the compositions with PA, prior to mixing platelets, the suspensions were milled for 21 hours. Next, the required amount of PA particles was added, and jar milled for 3 more hours. After completion of milling (total cycle time of 24 hours), an organic binder poly(2-ethyl 2-oxazoline) was added to the suspensions in a proportion of 5 wt.% of solids loading and jar milled further for 1 hour. Next, the suspensions were separated from grinding media and deaired for 30 minutes at low pressure in order to remove any trapped air bubbles. Although, platelet size before and after milling was not measured in this work, comparison from the SEM images did not indicate any change in the size of the PA particles.

This device consists of a thin steel plate ("Cold-finger") on which a hollow Teflon tube is placed and then the tube is filled with aqueous $Al_2O_3$ suspension. The dimensions of the Teflon tube are OD 19.5 mm, ID 11 mm, and height 28 mm. For each experiment, the mold was filled up to 20 mm height, i.e., was partially filled. Next, the Cold-finger is inserted inside a liquid nitrogen (L-$N_2$) Dewar for ice-templating. In this step, as the temperature of the Cold-finger decreases below 0 °C (freezing point of water), nucleation and growth of ice crystals start at the bottom of the suspension (in contact with the Cold-finger) and the crystals propagate upward under the influence of unidirectional temperature gradient. During each experiment, the top of the mold is kept open and exposed to room temperature. In this study, all the materials were fabricated at a

fixed gap (1 mm) in between the Cold-finger and L-$N_2$, which resulted in a comparable FFV across all the samples.

**Table S1**: Variation of longitudinal wave speed ($C_s$) and single transit time ($t_s$) as a function of composition.

| | UA-0PA | UA-2.5PA | UA-5PA | UA-10PA | UA-20PA | UA-25PA | UA-30PA |
|---|---|---|---|---|---|---|---|
| Wave speed, $C_s$ (m/s) | 635.6 | 827.4 | 960.5 | 1308.1 | 1410.4 | 1267.4 | 1277.3 |
| Transit time, $t_s$ (μs) | 3.1 | 2.4 | 2.1 | 1.5 | 1.4 | 1.6 | 1.57 |

**Table S2:** Variation of $\varepsilon_{cd}$, $e_{max}$ (%), $U_v$, and $U_m$ with composition and strain rate.

| | Composition | Strain rate | | | | |
|---|---|---|---|---|---|---|
| | | **$10^{-4}$/s** | **$10^{-3}$/s** | **$10^{-2}$/s** | **$10^{-1}$/s** | **$10^{3}$/s** |
| $\varepsilon_{cd}$ | UA-0PA | 0.33 ± 0.02 | 0.33 ± 0.02 | 0.33 ± 0.02 | 0.29 ± 0.01 | 0.44 |
| | UA-2.5PA | 0.34 ± 0.03 | 0.36 ± 0.02 | 0.37 ± 0.02 | 0.36 ± 0.02 | 0.53 ± 0.02 |
| | UA-5PA | 0.35 ± 0.01 | 0.36 ± 0.04 | 0.36 ± 0.01 | 0.34 ± 0.01 | 0.50 ± 0.03 |
| | UA-10PA | 0.35 ± 0.02 | 0.32 ± 0.02 | 0.34 ± 0.03 | 0.37 ± 0.03 | 0.49 ± 0.02 |
| | UA-20PA | 0.36 ± 0.02 | 0.37 ± 0.03 | 0.42 ± 0.04 | 0.37 ± 0.03 | 0.64 ± 0.04 |
| | UA-25PA | 0.4 ± 0.05 | 0.42 ± 0.03 | 0.39 ± 0.02 | 0.4 ± 0.03 | 0.61 ± 0.05 |
| | UA-30PA | 0.44 ± 0.02 | 0.45 ± 0.03 | 0.45 ± 0.03 | 0.44 ± 0.05 | 0.43 ± 0.11 |
| | | | | | | |
| $e_{max}$ (%) | UA-0PA | 85.10 ± 6 | 77.14 ± 7.1 | 82.9 ± 17.3 | 73.5 ± 14.8 | 87.19 |
| | UA-2.5PA | 72.1 ± 9.7 | 78.5 ± 9.7 | 82.2 ± 4.3 | 66.02 ± 6.3 | 93.39 |
| | UA-5PA | 75.4 ± 5.2 | 74.7 ± 6.9 | 63.3 ± 7.3 | 54.6 ± 3.02 | 83.6 ± 7.8 |
| | UA-10PA | 60.2 ± 4.3 | 66.3 ± 9.3 | 66.9 ± 18.1 | 56.5 ± 3.3 | 78.5 ± 5.2 |
| | UA-20PA | 74.9 ± 7.2 | 78.6 ± 11.6 | 77.4 ± 10.0 | 67.2 ± 13.7 | 92.8 ± 3.4 |
| | UA-25PA | 76.6 ± 4.7 | 82.4 ± 13.3 | 66.7 ± 8.7 | 69.3 ± 4.0 | 82.9 ± 11.3 |
| | UA-30PA | 53.8 ± 3.1 | 52.7 ± 3.6 | 52.5 ± 3.7 | 47.9 ± 4.3 | 72.3 ± 4.7 |
| | | | | | | |
| $U_v$ (MJ/m$^3$) | UA-0PA | 3.21 ± 0.11 | 3.55 ± 0.21 | 3.78 ± 0.39 | 4.04 ± 0.38 | 7.83 |
| | UA-2.5PA | 5.71 ± 1.5 | 6.97 ± 1.0 | 7.88 ± 1.2 | 7.09 ± 1.1 | 14.68 ± 1.0 |
| | UA-5PA | 7.67 ± 0.6 | 7.46 ± 2.3 | 9.40 ± 0.3 | 8.40 ± 0.5 | 19.79 ± 2.9 |
| | UA-10PA | 10.65 ± 2.0 | 10.51 ± 1.5 | 10.44 ± 3.2 | 12.27 ± 2.0 | 24.11 ± 1.5 |
| | UA-20PA | 17.98 ± 2.6 | 21.26 ± 4.3 | 26.14 ± 6.1 | 23.38 ± 5.8 | 62.88 ± 5.1 |
| | UA-25PA | 20.69 ± 7.2 | 24.79 ± 4.9 | 16.98 ± 2.6 | 23.41 ± 3.9 | 55.12 ± 6.2 |
| | UA-30PA | 23.63 ± 1.5 | 24.07 ± 1.6 | 26.62 ± 4.2 | 24.69 ± 4.4 | 32.67 ± 5.4 |
| | | | | | | |
| $U_m$ (kJ/kg) | UA-0PA | 2.68 ± 0.10 | 2.96 ± 0.18 | 3.11 ± 0.29 | 3.29 ± 0.36 | 6.33 |
| | UA-2.5PA | 5.17 ± 1.3 | 6.37 ± 1.0 | 7.0 ± 1.1 | 6.29 ± 1.0 | 13.46 ± 0.9 |
| | UA-5PA | 7.40 ± 0.6 | 7.13 ± 2.2 | 8.92 ± 0.3 | 7.91 ± 0.5 | 18.68 ± 2.8 |
| | UA-10PA | 10.74 ± 2.1 | 10.44 ± 1.5 | 10.28 ± 3.3 | 12.12 ± 1.8 | 23.69 ± 1.5 |
| | UA-20PA | 18.82 ± 2.6 | 22.41 ± 4.4 | 26.89 ± 6 | 23.44 ± 5.9 | 64.37 ± 6.9 |
| | UA-25PA | 22.49 ± 7.4 | 26.42 ± 5.4 | 17.92 ± 2.7 | 24.74 ± 4 | 59 ± 6.7 |
| | UA-30PA | 26.43 ± 1.6 | 26.7 ± 1.7 | 29.31 ± 4.7 | 27.22 ± 5.2 | 35.23 ± 6 |

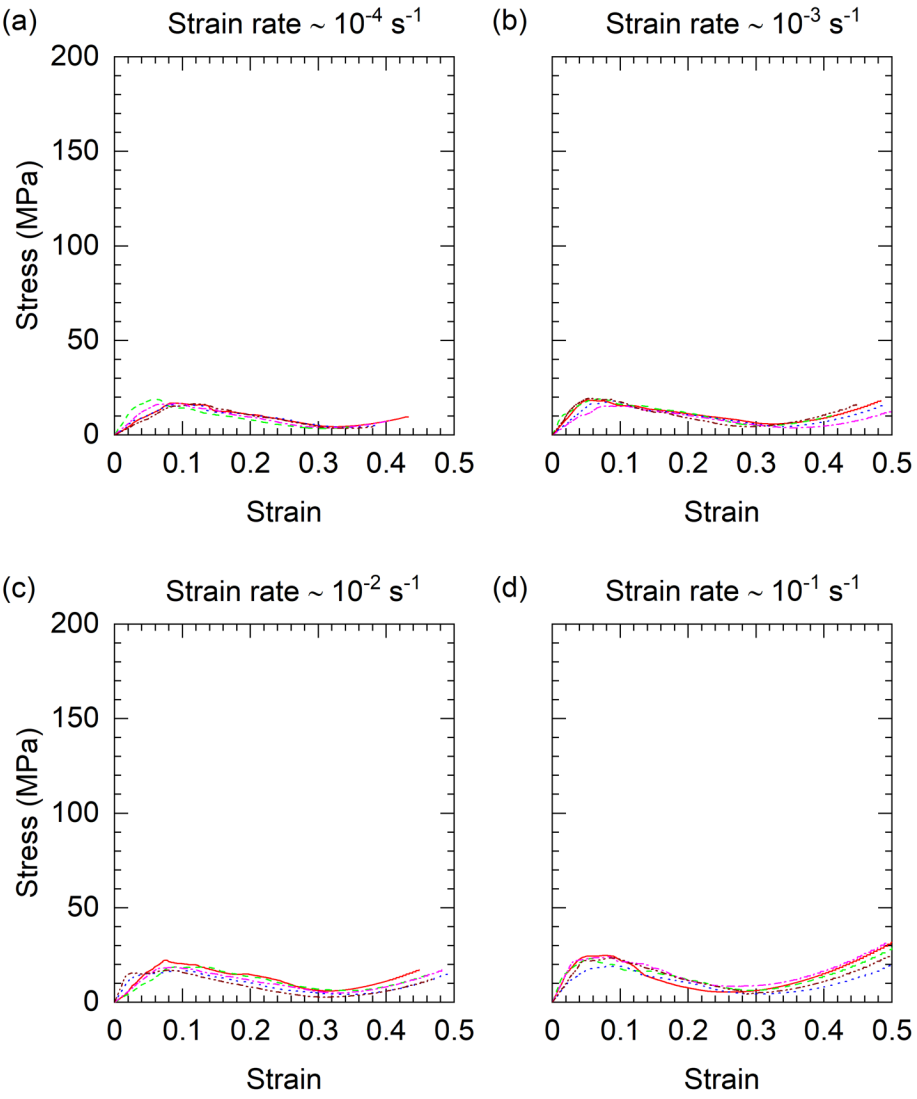


**Figure S1:** Quasistatic compressive stress-strain curves of UA-0PA material at (a) $10^{-4}$ $s^{-1}$, (b) $10^{-3}$ $s^{-1}$, (c) $10^{-2}$ $s^{-1}$, and (d) $10^{-1}$ $s^{-1}$ strain rates.

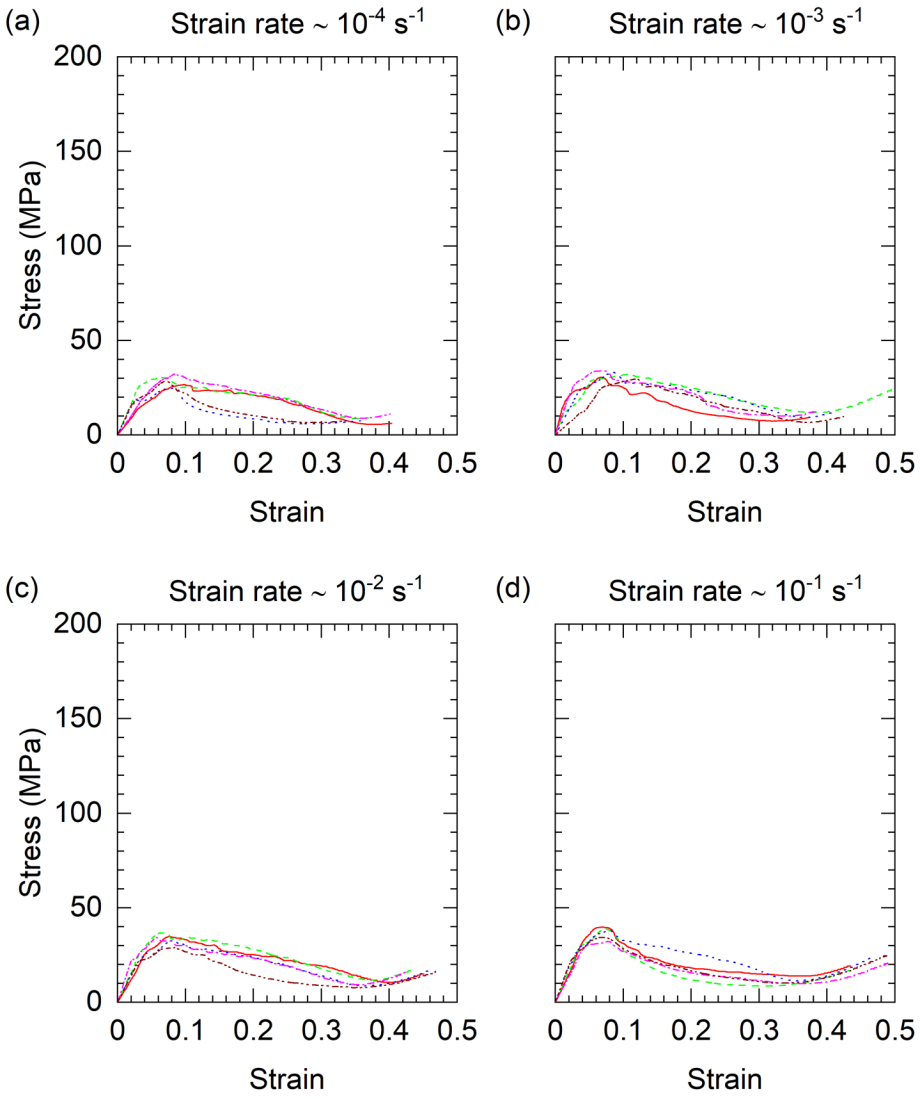


**Figure S2:** Quasistatic compressive stress-strain curves of UA-2.5PA material at (a) $10^{-4}$ $s^{-1}$, (b) $10^{-3}$ $s^{-1}$, (c) $10^{-2}$ $s^{-1}$, and (d) $10^{-1}$ $s^{-1}$ strain rates.

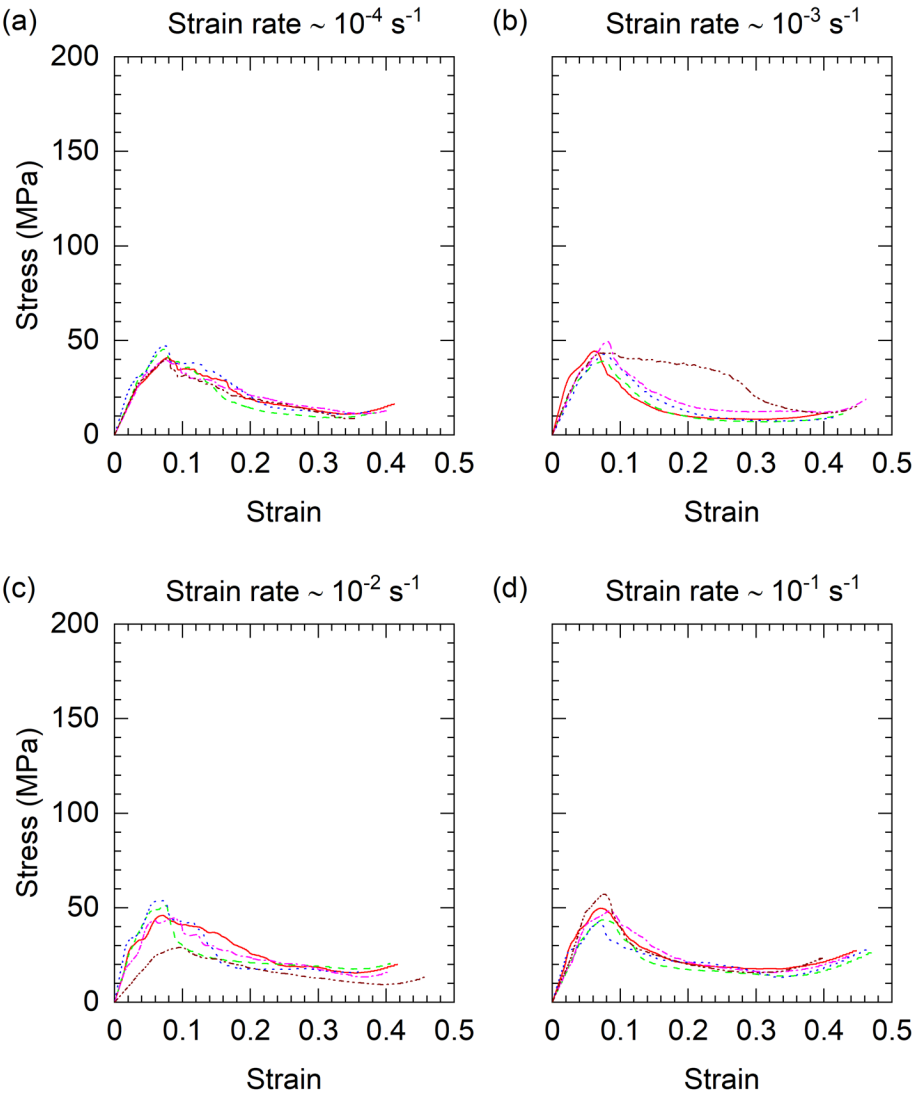


**Figure S3:** Quasistatic compressive stress-strain curves of UA-5PA material at (a) $10^{-4}$ $s^{-1}$, (b) $10^{-3}$ $s^{-1}$, (c) $10^{-2}$ $s^{-1}$, and (d) $10^{-1}$ $s^{-1}$ strain rates.

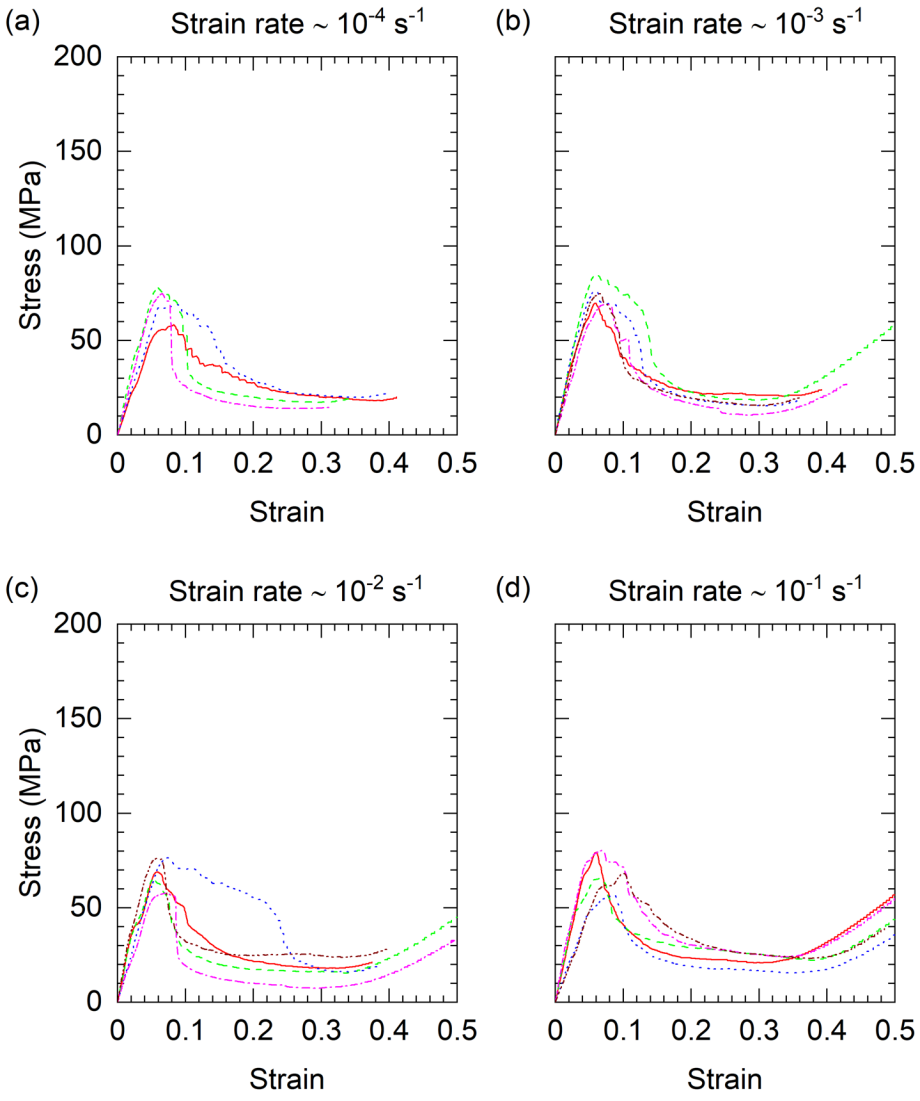


**Figure S4:** Quasistatic compressive stress-strain curves of UA-10PA material at (a) $10^{-4}$ $s^{-1}$, (b) $10^{-3}$ $s^{-1}$, (c) $10^{-2}$ $s^{-1}$, and (d) $10^{-1}$ $s^{-1}$ strain rates.

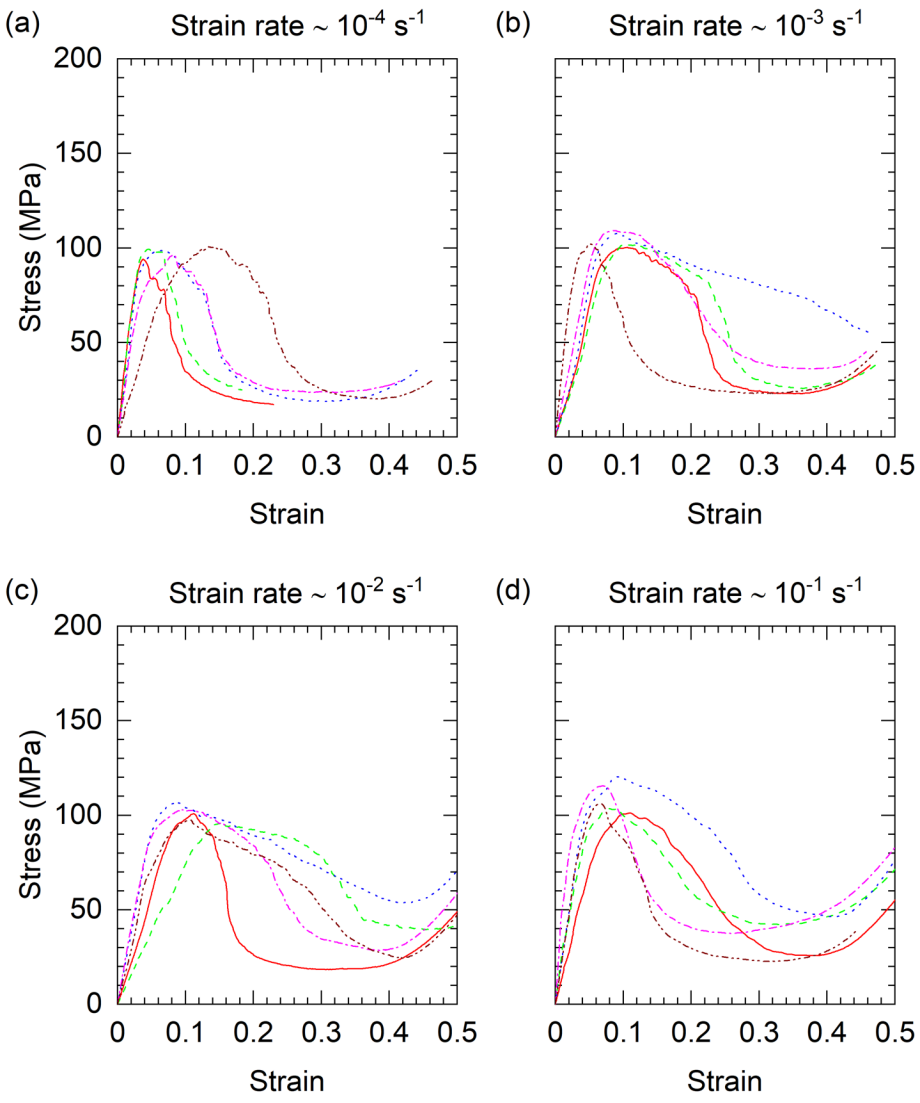


**Figure S5:** Quasistatic compressive stress-strain curves of UA-20PA material at (a) $10^{-4}$ $s^{-1}$, (b) $10^{-3}$ $s^{-1}$, (c) $10^{-2}$ $s^{-1}$, and (d) $10^{-1}$ $s^{-1}$ strain rates.

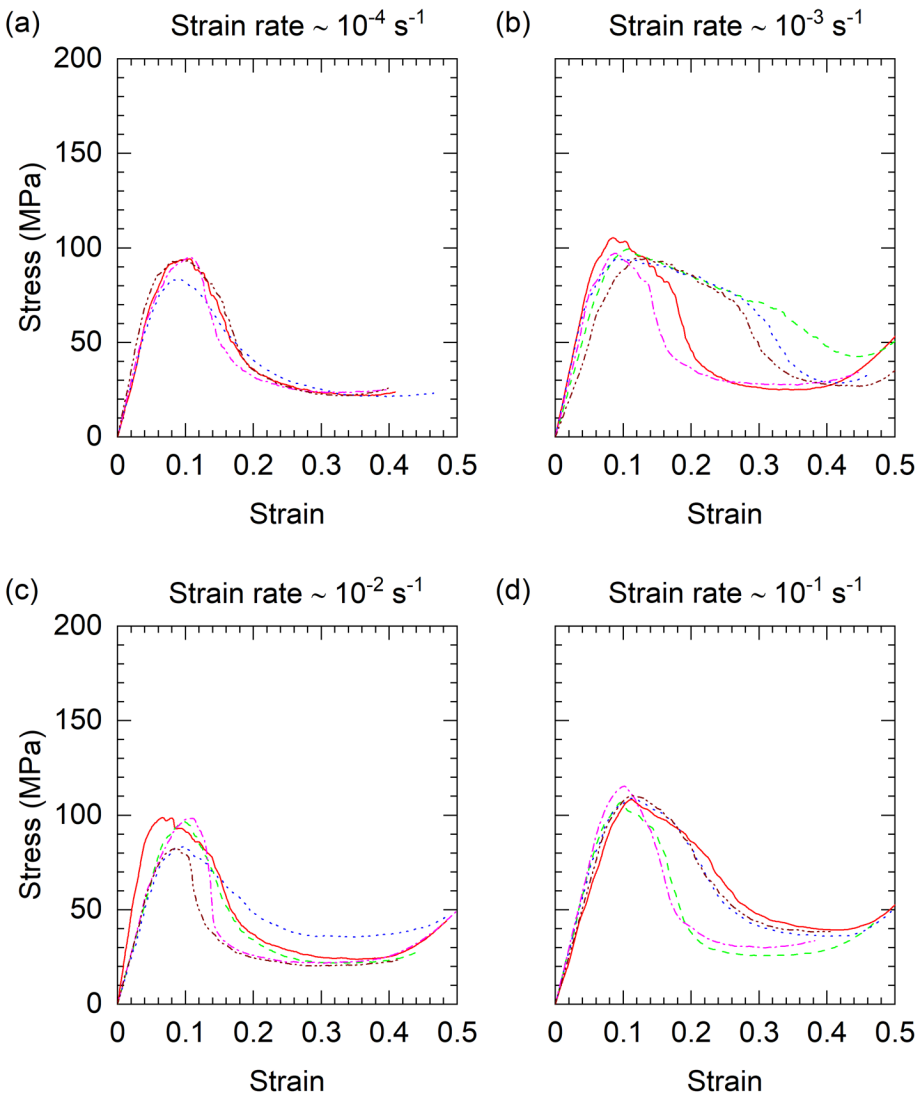


**Figure S6:** Quasistatic compressive stress-strain curves of UA-25PA material at (a) $10^{-4}$ $s^{-1}$, (b) $10^{-3}$ $s^{-1}$, (c) $10^{-2}$ $s^{-1}$, and (d) $10^{-1}$ $s^{-1}$ strain rates.

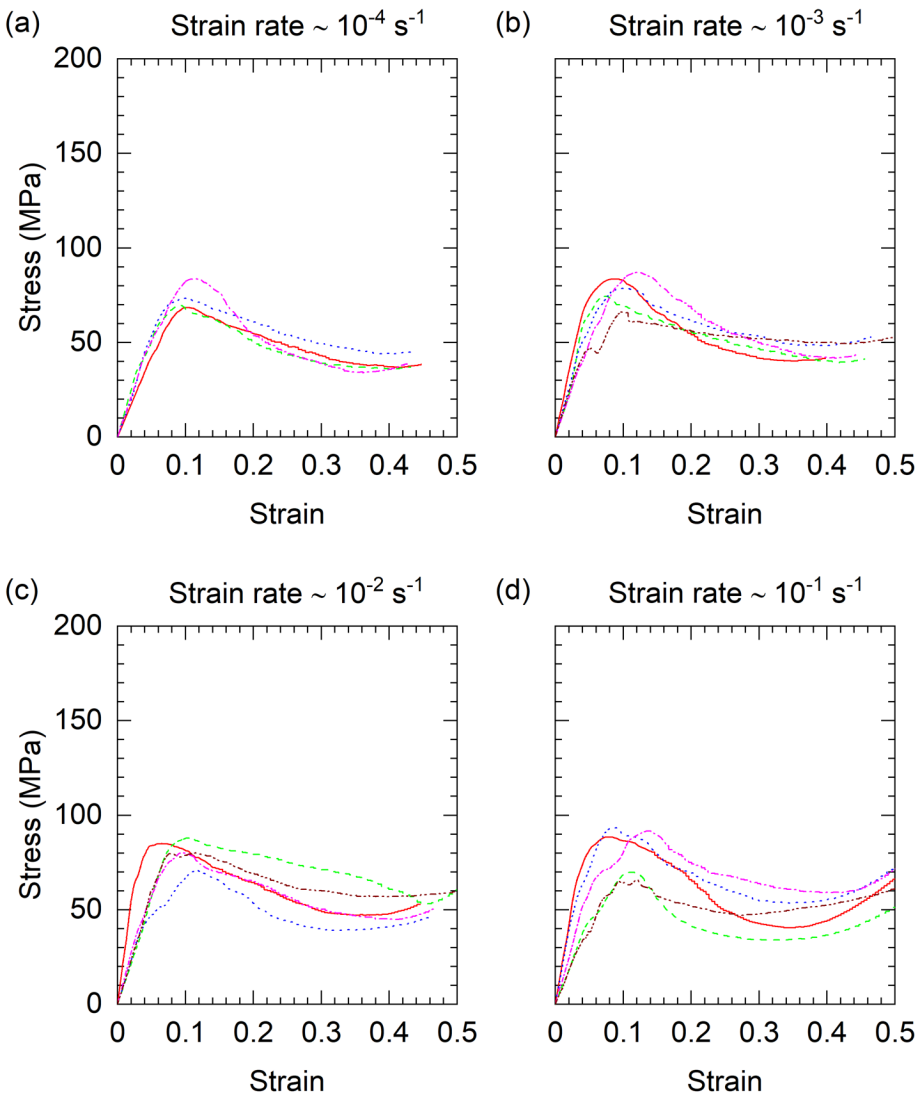


**Figure S7:** Quasistatic compressive stress-strain curves of UA-30PA material at (a) $10^{-4}$ $s^{-1}$, (b) $10^{-3}$ $s^{-1}$, (c) $10^{-2}$ $s^{-1}$, and (d) $10^{-1}$ $s^{-1}$ strain rates.

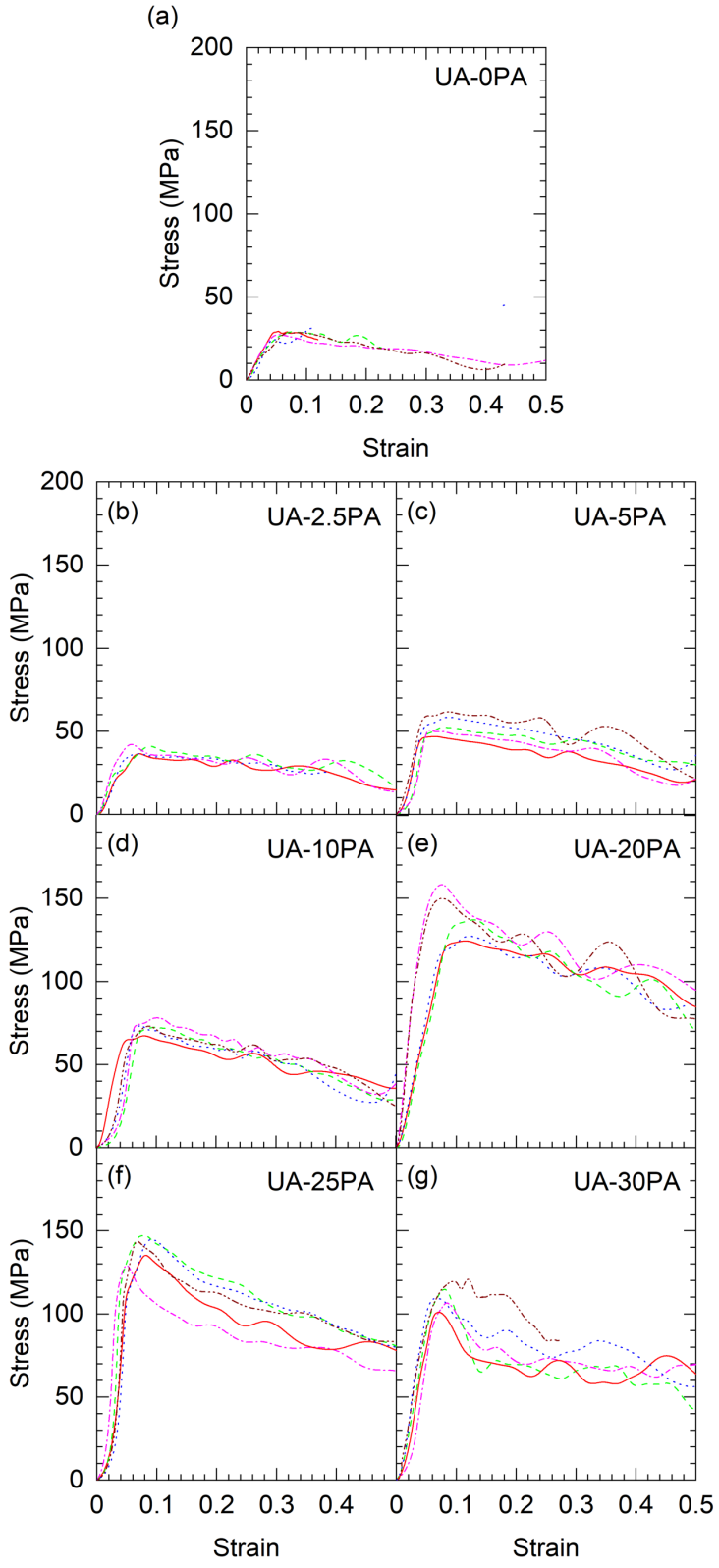


**Figure S8:** Dynamic compressive stress-strain curves of (a) UA-0PA, (b) UA-2.5PA, (c) UA-5PA, (d) UA-10PA, (e) UA-20PA, (f) UA-25PA, and (g) UA-30PA materials.